Creep deformation mechanisms in a γ Titanium Aluminide

Z. Abdallah, Rengen Ding, Nigel Martin, Mark Dixon, Martin Bache

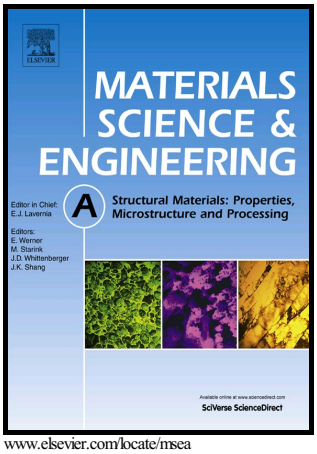

www.elsevier.com/locate/msea

PII: S0921-5093(16)30884-X
DOI: http://dx.doi.org/10.1016/j.msea.2016.07.109
Reference: MSA33940

To appear in: *Materials Science & Engineering A*

Received date: 2 June 2016
Revised date: 25 July 2016
Accepted date: 26 July 2016

Cite this article as: Z. Abdallah, Rengen Ding, Nigel Martin, Mark Dixon and Martin Bache, Creep deformation mechanisms in a γ Titanium Aluminide *Materials Science & Engineering A* http://dx.doi.org/10.1016/j.msea.2016.07.109

Creep deformation mechanisms in a γ Titanium Aluminide

Z. Abdallah[1*], Rengen Ding[2], Nigel Martin[3], Mark Dixon[3], Martin Bache[1]

[1] Institute of Structural Materials, College of Engineering, Bay Campus, Swansea University, Swansea SA1 8EN, UK.
[2] Interdisciplinary Research Centre in Materials, University of Birmingham, Edgbaston, Birmingham, B15 2TT, UK.
[3] Rolls-Royce plc, P.O. Box 31, Derby DE24 8BJ, UK.

Abstract

Titanium aluminides (TiAl) are considered as potential alternatives to replace nickel-based alloys of greater density for selected components within future gas turbine aero-engines. This is attributed to the high specific strength as well as the good oxidation resistance at elevated temperatures. The gamma (γ) titanium aluminide system Ti-45Al-2Mn-2Nb has previously demonstrated promising performance in terms of its physical and mechanical properties. The main aim of the current study, which is a continuation of a previously published paper, aims at evaluating the performance of this titanium aluminide system under high temperature creep conditions. Of particular interest, the paper is strongly demonstrating the precise capability of the Wilshire Equations technique in predicting the long-term creep behaviour of this alloy. Moreover, it presents a physically meaningful understanding of the various creep mechanisms expected under various testing conditions. To achieve this, two creep specimens, tested under distinctly different stress levels at 700^{o}C have been extensively examined. Detailed microstructural investigations and supporting transmission electron microscopy (TEM) have explored the differences in creep mechanisms active under the two stress regimes, with the deformation mechanisms correlated to Wilshire creep life prediction curves.

Keywords

Titanium aluminides, Intermetallics, Creep, Wilshire Equations, TEM.

1. Introduction

Titanium aluminides represent an important class of material due to their unique physical and mechanical properties, providing potential weight savings in gas turbine aero-engine components. Over thirty years of intensive research was conducted before titanium aluminides reached sufficient maturity for entry into service as critical rotating components in aircraft jet engines [1]. The ordered crystallography of this class of material provides attractive properties such as the high melting point, low density, high elastic modulus and low diffusion coefficient, in addition to good resistance to oxidation and corrosion. Titanium alumindes are superior in terms of their specific strength and temperature properties, in particular across the temperature range 500 to 900 ^{o}C, when compared to competing alloys such as conventional titanium, steel and nickel-based materials [2]. However, the shortfalls of this class of material are the low ductility (typically about 1% recorded at room temperature) alongside problematic formability and poor resistance to crack propagation.

Titanium aluminide alloys are categorised according to the content of the corresponding elements in the alloy with aluminium (Al) ranging between 45 and 48 (at. %) alongside the other elements which range between 1 and 10 (at. %), where the remaining balance of the alloy is titanium (Ti). Other constituent elements can be vanadium (V), chromium (Cr), manganese (Mn), niobium (Nb), tantalum (Ta) or molybdenum (Mo). Unique chemical compositions provide either a single phase γ-TiAl or a double phase γ-TiAl accompanied with α_2 (Ti_3Al). The single phase alloys typically contain Nb or Ta to improve the strength and oxidation resistance whereas the double phase alloys contain V, Cr or Mn to improve the ductility. The addition of boron (B) or magnesium (Mg) is to enhance the hot workability and formability of the alloy. To improve the creep performance of the alloy, tungsten (W) and/or carbon (C) are often added [2].

Four main sub-categories of titanium alumindes are recognised according to microstructural form, namely near-γ, duplex, near lamellar and fully lamellar. The fully lamellar and near lamellar variants, consisting of γ-phase along with small fractions of α_2-phase, exhibit superior creep resistance, fracture toughness and crack propagation resistance when compared to the duplex or near-γ variants. Due to the fact that future engine designs may employ titanium alumindes under creep dominated environments, the content of Al in such alloys is maintained around 46% (at. %) to provide the optimum static performance [2].

Extensive research has taken place over the past three decades to optimise intermetallic alloys with an acceptable level of ductility. The first significant advancement was achieved by introducing elements, such as niobium (Nb), that stabilise the β phase to attain reasonable levels of ambient temperature ductility and an improved creep performance and oxidation resistance when compared to other conventional titanium alloys [3], [4]. At the same time, the addition of manganese (Mn) has also resulted in an enhancement of the room temperature ductility [5]. Based on these findings, focus has been placed on alloys with an equivalent aluminium content ranging between 45 and 50%, with the system Ti-45Al-2Mn-2Nb, which has a fully lamellar microstructure, proving to be of particular interest towards service applications [6].

A previous assessment of creep behaviour has been published from this laboratory on the system Ti-45Al-2Mn-2Nb [7]. The current investigation was designed to extend our understanding of the various creep deformation mechanisms activated under different regimes of applied stress and therefore implicated in generating extremes in rupture life.

2. Characterisation Procedures

The selected TiAl intermetallic alloy, Ti-45Al-2Mn-2Nb (containing 0.8 vol. %TiB_2 to control grain refinement), was supplied in the cast and HIP'ed condition with a fully lamellar microstructure. Cylindrical creep specimens were machined from the stock material with a finished diameter of 5.6mm and a gauge length of 28.0mm. Creep testing was carried out according to the guidelines of the ISO 204 standard but utilising constant-stress machines at temperatures in the range 625-750^{o}C and stresses between 150 and 550MPa. The elongation of specimens during the test was monitored using dual averaging parallel extensometers which

employ high precision LVDTs. The specimen temperature was measured using calibrated type-R thermocouples. A full description of the equipment employed in the current research paper can be found elsewhere [8]. For the scanning electron microscopy (SEM) investigations, the samples were sectioned on an orthogonal plane relative to the fracture surface. This allowed the examination of the fracture surface features and underlying grain morphology. The optical microscopy (OP) samples were auto-polished using 220 MD-Piano, MD-Plan and MD-Chem discs with the aid of suspension polishing liquids to produce a mirror-like finish. The microstructure was then revealed using a solution of H_2O (25ml) + HNO_3 (25ml) + HF (2ml) + glycerine (50ml) on the polished surfaces. In order to investigate the creep deformation mechanisms, transmission electron microscopy (TEM) observations were carried out on a FEI Tecnai F20 operating at 200 kV. Flat TEM discs of 0.2 mm thickness and 3mm diameter were sectioned perpendicular to the axial length of the crept specimens in addition to untested specimens for comparison. These discs were then thinned to perforation using a twin jet electro-polisher in 5% perchloric acid, 35% butanol and 60% methanol solution at – 30°C with an applied voltage of 25 V.

3. Creep Modelling

Full creep curves were generated from the individual tests allowing the time to fracture, creep ductility and the minimum creep rate properties to be defined. In a previously published paper [7], the Wilshire Equations technique was employed to model the creep behaviour of the same intermetallic alloy. The predictions were reasonably accurate with the time to fracture and minimum creep rate properties precisely estimated using this model. In addition, as part of the current paper is data from the longest test carried out during this programme of work, with a total creep life of 9,182 hours (almost 13 months) measured at 190MPa and 700^{o}C. The main aim of this long-term test was to confirm whether this data point could be predicted via extrapolation of the previous, relatively shorter life creep data generated through analysis based on the Wilshire model.

Furthermore, the specimen relating to this long-term result along with the shortest term specimen, both tested at 700^{o}C, would be the focus of detailed characterisation to describe the creep deformation and failure mechanisms. With reference to the Wilshire stress-rupture predictions, see Figure 3, these two specimens deliberately fall above and below the distinct “kink” in the curves, a point that divides the isothermal curves into “high” (upper-left) and “low” (bottom-right) stress regimes distinguished by different slopes. It was postulated that the two regimes may correspond to different creep deformation mechanisms. It has been found during previous studies, assessing the conventional titanium alloy Timetal 834 as well as Ti-45Al-2Mn-2Nb, that the ‘kink’ point approximately correlates to the bulk yield stress of the material, which implies that varying creep mechanisms are taking place within the upper and lower regimes, [9], [7].

4. Results

The microstructure of the alloy, revealed after etching, showed a fully lamellar nature, Figure 1. In this context, the grain (or colony) is defined as the region where the lamellae have the same alignment. The colony boundaries contain interlocking, overlapping lamellae imparting additional strength to the boundaries during deformation of the material. The spacing between the lamellae will influence the creep behaviour, confirmed elsewhere [10]. The measured average colony size of the current material was approximately 90μm, similar to the material assessed by [11] .

Full creep curves, i.e. strain versus time, were obtained with distinctive primary, secondary and tertiary stages, Figure 2. The primary region is the area of a decaying creep rate on the contrary to the tertiary stage which is characterised by accelerating creep deformation [12]. These curves provide information on the creep life when the sample ruptures, t_r, alongside the total creep ductility, ε_r, of the alloy. The slope at any point along the curve, $\dot{\varepsilon}$, is defined as the strain rate at that particular point which can be evaluated by dividing the change in strain by the change in time ($\dot{\varepsilon} = d\varepsilon/dt$), Figure 2. Generally, the creep rate in the primary region decreases, remains constant in the secondary region, or sometimes reaches a minimum value which is called the minimum creep rate $\dot{\varepsilon}_m$, and then finally increases throughout the tertiary region leading on to fracture. The creep life, t_r, was found to be inversely proportional to stress, σ, and temperature, T, unlike the strain rate, $\dot{\varepsilon}$, which is always proportional to either increase in σ or T [13], (Wilshire & Evans, 1993).

The relationship between σ, T, t_r and $\dot{\varepsilon}$ is defined by the power law equation:

$$1/t_r \propto \dot{\varepsilon}_m = A\,\sigma^n \exp(-Q_c/RT) \qquad \text{.....(1)}$$

where A is a material constant, n is the stress exponent, Q_c is the minimum amount of energy required to initiate creep (i.e. activation energy) and R is the gas constant (8.314 J/mol K). It was found elsewhere [7] that the value of the stress exponent (n) for this material lies between 5 and 7 (for temperatures 675-750^{o}C at low stress level) and between 8 and 11 (for temperatures 625-650^{o}C at high stress level). Similarly, it has been found that the value of the activation energy (Qc) varied between ~ 255 to ~ 520 kJ/mol K. This suggests that the variability of such 'constants' reveals that there might be a change in creep mechanism with changing conditions from high to low stress regimes at varying testing temperatures. These findings formed the rationale for the current paper, i.e. the selection of two specimens, both tested at 700^{o}C but under two extreme loading conditions (the lowest and highest applied stress) in order to compare their creep behaviour.

4.1 Stress-Rupture Results

Great emphasis is placed upon the development of a predictive tool capable of precisely forecasting the stress rupture behaviour of materials using simple and physically meaningful

equations. There have been extensive efforts in this area of research applying numerous predictive techniques to titanium alumindes, steels and titanium alloys [7], [14] and [15]. The results obtained in these studies have shown that the physical creep behaviour has been simulated and predicted well using the Wilshire Equations technique [16] :

$$\sigma/\sigma_{TS} = \exp\left(-k_1 \left[t_f \exp\left(-Q_c^*/RT\right)\right]^u\right)$$

where σ is the applied stress, σ_{TS} is the ultimate tensile strength, k_1 and u are fitting constants, t_f is the time to fracture, Q_c* is the activation energy for creep that is obtained at constant σ/σ_{TS}, R is the gas constant and T is the applied temperature. It is worthwhile mentioning that detailed procedures for evaluating the value of k_1, u and Q_c* are published elsewhere [9], [7]. The results obtained in a former study [7] using the predictions of the Wilshire Equations technique are shown in Figure 3.

Since a previous publication in 2013, a long term test conducted at a stress of 190MPa has reached completion. The data point relating to this specimen is superimposed on Figure 3. It is noted that it corresponds well to the previously predicted stress-rupture trend curve. This specimen plus that relating to the test performed at 375MPa at the same temperature of 700^{o}C are circled as the specimens selected for detailed characterisation, given that they lie below and above the associated “kink” point in the prediction curve respectively.

4.2 Characterisation of high and low stress regime specimens tested at 700^{o}C

4.2.1 Creep Curves

Full creep curves were recorded for the two specimens as shown in Figure 4. Due to the significant variation in creep life between these two samples (354 and 9,182 hours), the curves are plotted on a log-scale graph in order to illustrate the comparable shapes of the curves. The ductility achieved at the higher stress level was slightly larger than that achieved at the lower stress. In this format it is difficult to differentiate the various stages of each creep curve, i.e. the decaying primary, steady state secondary and accelerating tertiary stages. This can better be demonstrated by plotting the strain rate, at each point along the original creep curves, against the corresponding time as shown in Figure 5.

It can be seen that the primary stage (i.e. decaying strain rate) persists for approximately 10% of the total creep life recorded for the high stress specimen at 375MPa in comparison to more than 50% for the test performed at 190MPa.

This suggests that the specimen tested at 190MPa experienced strain hardening for the majority of its life (i.e. a higher dislocation density is expected within the microstructure). There is no significant secondary (recovery) stage relating to this test which suggests that any newly generated dislocations may not be annihilated during ongoing creep. At the higher stress level, it could be expected that a relatively higher dislocation density would prevail, however, from Figure 5, it is apparent that a period of recovery occurs during which dislocations could be annihilated. At the relatively high stress level, even though more dislocations may be

generated the spacing between them would be shorter which facilitates their subsequent annihilation (and vice versa at the lower stress level. This infers that the movement and annihilation of dislocations at the higher stress level is more rapid than that at the lower stress level. This theory will be supported by the TEM results to follow.

4.2.2 Optical Microscopy

Optical images taken from the two crept samples are shown in Figure 6. It was noted that the higher stress sample contained more interlamellar and intercolony cracking than that at the lower stress level. These internal cracks would accelerate the creep fracture mechanism and induce a shorter life when compared to the lower stress sample. This infers that a relatively large proportion of the strain damage is consumed in moving the colonies and the lamellae apart from each other rather than generating intra-colony dislocations. In contrast, strain accumulation in the low stress sample was presumably largely due to a process of generating and moving dislocations. The lack of recovery noted at this lower stress level (Figure 5) may suggest dislocations increase in density and interact, increasing the creep resistance and characterised by the decreasing strain rate observed in this sample.

4.2.3 Scanning Electron Microscopy

Scanning electron microscopy (SEM) images are shown in Figure 7. It is apparent that there is a difference in fracture appearance between the two samples. The higher stress sample showed a rougher fracture surface resulting from interlamellar and translamellar cracking and delamination of the lamellar structure (facets). This correlates to the internal cracking between the lamellae colonies as observed in Figure 6. In contrast, the lower stress sample showed a relatively ductile, dimpled fracture surface with fewer facets. Fracture in this sample, however, continues to focus along the grain boundaries.

4.2.4 Transmission Electron Microscopy

Transmission electron microscopy (TEM) images are shown in Figure 8. For comparison, an image from the parent, un-tested material is illustrated, taken under a bright field many-beam condition wherein only low density dislocations can be seen. These must be the inherent dislocations formed during casting and lamellar transformation that have survived the post-cast HIPping and heat treatment. Alongside the above, dislocations might have been formed during the mechanical preparation of the foils prior to TEM examination. In comparison, the specimen crept at 700°C and 190MPa has a denser dislocation structure when viewed in a bright field two-beam image. The beam direction is close to [1-10] and the operating vector is g = (111), identical to that employed for similar investigations [17]. Under such two-beam conditions, some dislocations could lack contrast, however, those in contrast still indicate a high dislocation density. This leads to the conclusion that creep deformation has taken place extensively through dislocation gliding and climbing under these conditions. Detailed observation reveals dislocations are elongated and pinned at many locations along their

length. Moreover, the segments on either side of these pinning points are significantly bowed. This may be due to the presence of jogs or extrinsic pinning due to fine precipitates such as oxides, etc. This behaviour has also been observed in other studies on intermetallic TiAl alloys [17].

The TEM image taken from the sample tested at 375MPa and 700°C is significantly different. In addition to a relatively higher dislocation density with less pinning and bowing, it is evident that twinning is a prominent feature at this condition. This is apparent in the bright field two-beam TEM image in which a high density of twins can be seen across γ lamellae. Twinning in crept TiAl alloys has long been observed [18]. However, there has been no systematic study on the relationship between twinning and creep deformation parameters. Hsiung et al. [18] reported observations of twinning in lamellar TiAl alloys crept at both low and high stress levels but twinning only commenced once deformation entered the secondary creep stage, indicating that that twinning is a strain-related phenomenon. Other workers have suggested that a critical combination of high creep stress and sufficient creep strain encourages the formation of twins [19], [20]. In the present study, it is pertinent to note the relatively higher levels of ductility observed within the high stress regime, Figure 4, and the associated prevalence of twinning. Twins have also been implicated as the preferential site for creep crack initiation and subsequent propagation [21], consistent with the propensity of inter-colony cracking detected during the present study for the specimen tested at high stress.

5. Discussion

Firstly, in terms of mechanical performance, it was encouraging to note that the rupture life measured from the recently completed long-term creep test fell precisely on the Wilshire curve formerly predicted for this specific test temperature (700^{o}C), Figure 3. This provides further evidence of the capability of the Wilshire technique in predicting such long-term creep behaviour for a wide range of metallic alloys. This long-term result fell within the low stress regime indicated by the Wilshire prediction, hence the decision to select this specimen to compare to a counterpart tested at relatively high stress with respect to potential differences in deformation mechanism.

It is recognised that the TEM samples taken from the two specimens characterised during the present exercise provide a limited database from which to determine the creep mechanisms active across a range of stress and temperature conditions in the gamma titanium aluminide Ti-45Al-2Mn-2Nb. In addition, these have only provided post mortem inspections of dislocation structures as they were developed immediately prior to creep rupture and not throughout various stages of the creep life. For a full description of the creep mechanisms active across the stress regimes, multiple interrupted tests would be required, a task beyond the scope of the present work. Within these limitations, however, distinct differences in dislocation structures have been illustrated for the parent (untested) alloy and specimens subjected to relatively low and high stress conditions at 700^{o}C. Of particular interest, this validates our original assumption that creep mechanisms differ in the regimes either side of the ‘kink’ in the Wilshire prediction curves, a point which typically corresponds to the bulk yield stress.

The individual creep tests have demonstrated classical creep deformation behaviour, characterised by primary, secondary and tertiary stages, Figure 4. The extent of each stage, however, was dependent on the creep conditions imposed and such behaviour is consistent with previous reports, [22]. For instance, the low stress test was dominated by primary creep contributing approximately 50% of the total creep life, in stark contrast to only 10% primary creep contribution at the high stress level, Figure 4 and Figure 5. Variations in the activation energy (Q_c) and stress exponent (n) calculated for individual tests by use of the power law equation (equation 1) have been noted, [7]. The activation energy and stress exponent are generally proportional to the applied stress level. There is a strong understanding that high activation energy and stress exponent values are indicative of 'dislocation' creep, whereas low values of these two parameters represent 'boundary diffusion' creep [23]. Irrespective, the results obtained from the present study revealed that dislocation formation and twinning are the most dominant creep mechanisms at the low and high stress regimes respectively, with no evidence of diffusion creep mechanisms detected.

The microstructure of the TiAl alloy, Figure 1, showed a fully lamellar microstructure characterised by lamellar colonies forming grains of various orientations. The spacing of the lamellae has a direct inverse proportionality relative to the creep resistance - i.e. smaller spacing provides greater creep resistance, [10]. The grain boundaries show an interactive zone whereby the ends of lamellae overlap and interlock in such a way that provides an additional resistance against sliding and intergranular fracture. Optical inspections, Figure 6, showed two distinct fracture behaviours. The sample crept at the higher stress showed significantly greater inter-colony cracking suggesting that a large proportion of the strain accumulated at this condition was consumed in separating the colonies apart. In a study by Zhu et al. [10] on a similar alloy, it was confirmed that the α_2 (Ti_3Al) phase accumulates along grain boundaries during creep deformation. Since this phase is more brittle than the surrounding γ phase [24], it is more susceptible to fracture under high stresses leading to inter-colony cavities along the grain boundaries. The model suggested by Zhu et al. [10] is reproduced in Figure 9. The current SEM images suggest that a similar mechanism of intergranular brittle fracture, characterised by the facet formation resulting from the delamination of the lamellar microstructure. The fracture at the lower stress level appeared relatively ductile and characterised by dimple features.

In Figure 8, it can be clearly seen that the dislocations were curved and randomly distributed within the structure, within gamma and α_2 laths. The dislocations have mostly been generated at the lamellar interfaces and grain boundaries as observed in other studies on TiAl alloys [25]. The nature of the dislocations, in terms of bowing and pinning, has also been observed in TiAl [17]. The parallel twinning that occurs in TiAl under creep results in the refinement of the lamellar microstructure and leads to subsequent strengthening of the alloy [26]. Here, the term 'parallel' twinning refers to the mechanism whereby twinning takes place along the {111} direction, i.e. the lamellar boundaries, and this results in the creation of additional γ plates parallel to the original lamellar boundaries. A study on creep effects in lamellar microstructures [27] revealed that twinning mechanisms contribute greatest to the deformation in the early stages of creep, or under short-term / high stress creep conditions, in a similar fashion to that observed in the current study. It was also concluded that the higher the applied stress the

lower the spacing between the lamellae which confirmed that twinning was more pronounced at higher stress levels.

6. Conclusions

The following high level conclusions can be drawn from the present study:

- The γ-TiAl alloy Ti-45Al-2Mn-2Nb exhibited classical creep behaviour characterised by primary, secondary and tertiary creep stages before fracture.
- The Wilshire Equations technique proved capable of predicting the long-term creep behaviour of this alloy.
- TEM investigations demonstrated distinct creep mechanisms active above and below the Wilshire prediction "kink".
- Dislocation creep was prevalent within the low stress regime and twinning of the lamellae at high stress.

Acknowledgments

The current research was conducted under the Technology Strategy Board (TSB) contract SILOET (AB266C/4). The financial and technical support from TSB and Rolls-Royce plc is acknowledged.

References

[1] F. H. J. O. M. Appel, Gamma Titanium ALuminide Alloys: Science and Technology, Wiley-VCH Verlag GmbH, 2011.
[2] J. Lapin, "TiAl-Based Alloys: Present Status and Future Perspectives," *Metal 2009,* no. http://metal2013.tanger.cz/files/proceedings/metal_09/Lists/Papers/077.pdf, 2009.
[3] J. M. S. S. W. McBride, "Modelling Tensile Properties of Gamma-Based Titanium Aluminides Using Artificial Neural Network," *Materials Science and Engineering A,* vol. 384, pp. 129 - 137, 2004.
[4] S. W. M. Kerry, "Creep Behaviour of Ti3Al-Based Titanium Aluminide Alloys Containing Molybdenum," *Materials Science and Engineering A,* Vols. 192 - 193, pp. 856 - 861, 1995.
[5] W. M. C. L. K. H. S. Soboyejo, "An Investigation of the Fatigue and Fracture Behavior of Mn-Containing Gamma Titanium Aluminides," *Metallurgical and MAterials Transactions A,* vol. 26A, no. 9, pp. 2275 - 2291, 1995.
[6] M. B. C. V. W. Bache, "Characterisation of Foreign Object Damage and Fatigue Strength in Titanium Based Aerofoil Alloys," *Materials Science and Engineering A,* vol. 354, pp. 199 - 206, 2003.
[7] Z. W. M. B. M. Abdallah, "High Temperature Creep Behaviour in the γ Titanium Aluminide Ti–45Al–2Mn–2Nb," *Intermetallics,* vol. 38, pp. 55 - 62, 2013.
[8] B. E. R. Wilshire, Introduction to Creep, London: The Institute of Materials, 1993.

[9] Z. P. K. W. S. Abdallah, “Advances in the Wilshire extrapolation technique - Full creep curve representation for the aerospace alloy Titanium 834,” *Materials Science and Engineering: A,* vol. 550, pp. 176 - 182, 2012.
[10] H. S. D. M. K. A. P. Zhu, “Grain Boundary Morphology and Its Effect on Creep of TiAl Alloys,” *Materials Transactions,* vol. 45, no. 12, pp. 3343 - 3348, 2004.
[11] H. S. D. M. K. Zhu, “Microstructural Characteristics and Creep Behavior of 45XD TiAl Alloys,” vol. 45, no. 8, 2004.
[12] Y. Haddad, Mechanical Behaviour of Engineering Materials, Netherlands: Kluwer Academic Publishers, 2000.
[13] K. A. H. Naumenko, Modeling of Creep for Structural Analysis, Berlin: Springer, 2007.
[14] W. A. Z. W. M. Harrison, “A Model for Creep and Creep Damage in the γ-Titanium Aluminide Ti-45Al-2Mn-2Nb,” *Materials,* vol. 7, no. 3, pp. 2194-2209, 2014.
[15] Z. G. V. W. M. P. K. Abdallah, “A Critical Analysis of the Conventionally Employed Creep Lifing Methods,” *Materials,* vol. 7, no. 5, pp. 3371-3398, 2014.
[16] B. S. P. Wilshire, “A new methodology for analysis of creep and creep fracture data for 9–12% chromium steels,” *International Materials Reviews,* vol. 53, no. 2, pp. 91-104, 2008.
[17] G. V. V. M. M. Viswanathan, “MODIFICATION OF THE JOGGED-SCREW MODEL FOR CREEP OF GAMMA-TiAl,” *Acta Materialia,* vol. 47, no. 5, pp. 1399 - 1411, 1999.
[18] L. N. T. C. B. W. J. Hsiung, “Interfacial Dislocations and Deformation Twinning in Fully Lamellar TiAl,” *Materials Science and Engineering A329-331,* vol. 329–331, pp. 637 - 643, 2002.
[19] Z. B. T. Jin, “ High-Temperature Ordered Intermetallic Alloys,” Pennsylvania, 1992.
[20] M. L. M. Morris, “Deformed Microstructures During Creep of TiAl Alloys: Role of Mechanical Twinning,” *Intermetallics,* vol. 5, pp. 339 - 354, 1997.
[21] V. S. N. Stoloff, Physical Metallurgy and processing of Intermetallic Compounds, Chapman & Hall, 1996.
[22] G. M. M. L. V. Angella, “Analysis of creep behaviour of TiAl-8Ta intermetallic alloy,” 2010.
[23] R. M. P. Hayes, “TENSION CREEP OF WROUGHT SINGLE PHASE GAMMA TiAl,” *Acta Metallurgica et Materialia,* vol. 43, no. 7, pp. 2761 - 2772, 1995.
[24] M. A. V. Arenas, “Analysis of Gamma Titanium Aluminide Welds Produced by Gas Tungsten Arc Welding,” *Welding Research,* pp. 110 - 115, 2003.
[25] W. D. S. Zhang, “The controlling creep processes in TiAl alloys at low and high stresses,” *Intermetallics,* vol. 10, no. 6, pp. 603 - 611, 2002.
[26] F. W. R. Appel, “Transgranular Cleavage Fracture of Fe3Al Intermetallics Induced By Moisture and Aqueous Environments,” *Materials Science and Engineering,* vol. R22, pp. 187 - 195, 1998.
[27] H. M. K. Kim, “Changes in Lamellar Microscture by Parallel Twinning During Creep in Soft Crystal of TiAl Alloy,” *Tnasactions of Nonferrous Metals Society of China,* vol. 12, no. 4, pp. 561 - 568, 2002.
[28] T. Materia, “Creep and Stress Rupture Properties,” 2015. [Online]. Available: http://www.totalmateria.com/page.aspx?ID=CheckArticle&site=kts&NM=296. [Accessed 8 6 2015].
[29] R. F. A. T. U. Viswanathan, “Creep-Resistant Steels,” Woodhead Publishing Limited, 2008, pp. 549 - 551.

Figure 1: Microstructure of the cast and HIP'ed Ti-45Al-2Mn-2Nb alloy.

Figure 2: A typical creep curve for Ti-45Al-2Mn-2Nb at 675^{o}C and 450MPa (left) and the various stages of the typical creep curve (right), **(Wilshire & Evans, 1993).**

Figure 3: The Wilshire predictive curves applied to Ti-45Al-2Mn-2Nb creep data **(Abdallah, 2013)**, highlighting the additional data point measured at 700^{o}C and 190MPa plus the two specimens selected for characterisation (circled).

Figure 4: Full creep curves for the two selected tests at 375MPa and 190MPa, both at 700^{o}C.

Figure 5: Strain rate plotted against time for the two selected tests at 375MPa and 190MPa, both at 700^{o}C.

Figure 6: Optical micrographs of the samples tested at 375MPa (left) and 190MPa (right), both at 700^{o}C.

Figure 7: Scanning electron microscopy images of the samples tested at 375MPa (left) and 190MPa (right), both at 700^{o}C.

Figure 8: Transmission electron microscopy (TEM) of the parent material (left) and the two crept specimens at 375MPa (middle) and 190MPa (right).

Figure 9: A model of creep deformation in TiAl alloys **(Zhu, 2004)**.

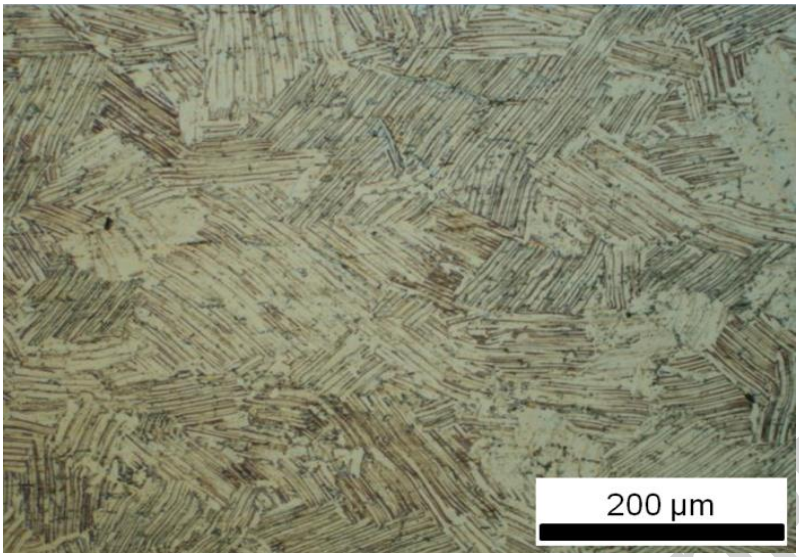

Figure 1: Microstructure of the cast and HIP'ed Ti-45Al-2Mn-2Nb alloy.

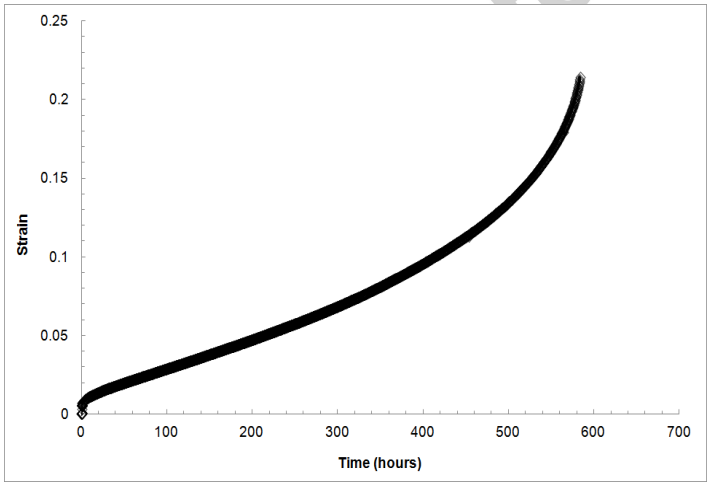

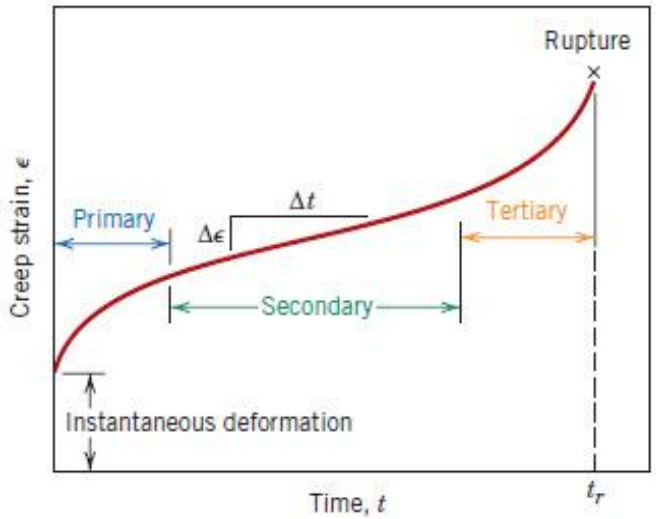

Figure 2: A typical creep curve for Ti-45Al-2Mn-2Nb at 675^{o}C and 450MPa (left) and the various stages of the typical creep curve (right), **(Wilshire & Evans, 1993).**

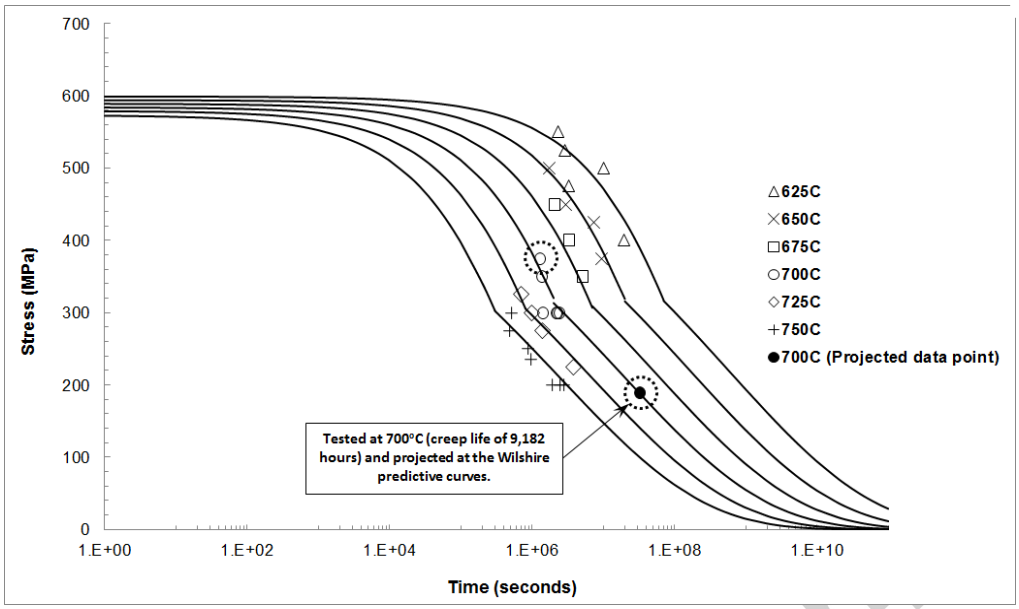

Figure 3: The Wilshire predictive curves applied to Ti-45Al-2Mn-2Nb creep data **(Abdallah, 2013)**, highlighting the additional data point measured at 700°C and 190MPa plus the two specimens selected for characterisation (circled).

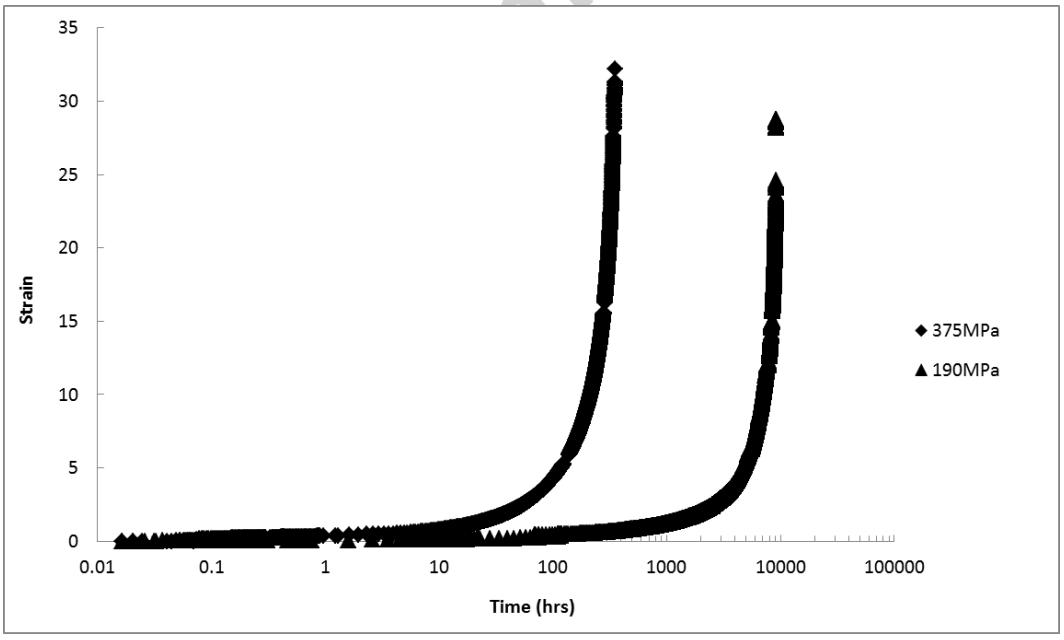

Figure 4: Full creep curves for the two selected tests at 375MPa and 190MPa, both at 700°C.

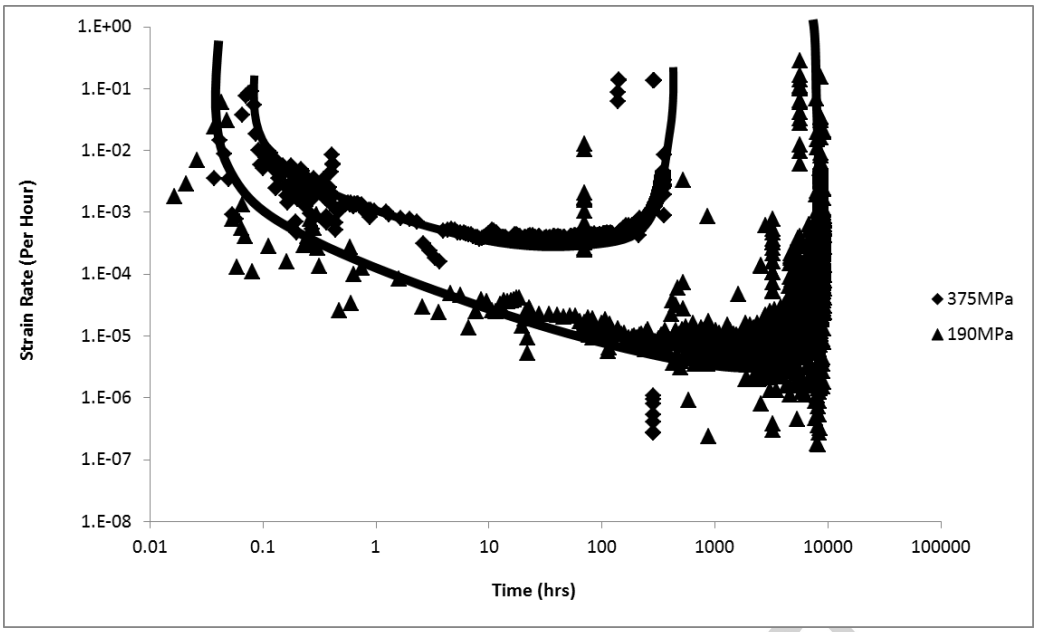

Figure 5: Strain rate plotted against time for the two selected tests at 375MPa and 190MPa, both at 700°C.

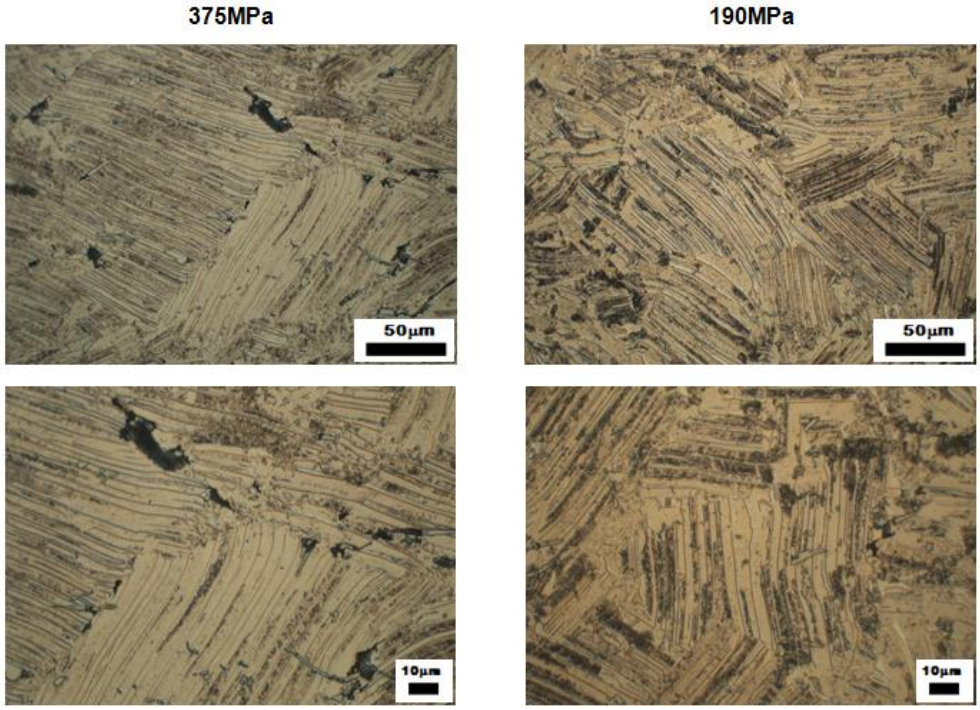

Figure 6: Optical micrographs of the samples tested at 375MPa (left) and 190MPa (right), both at 700°C.

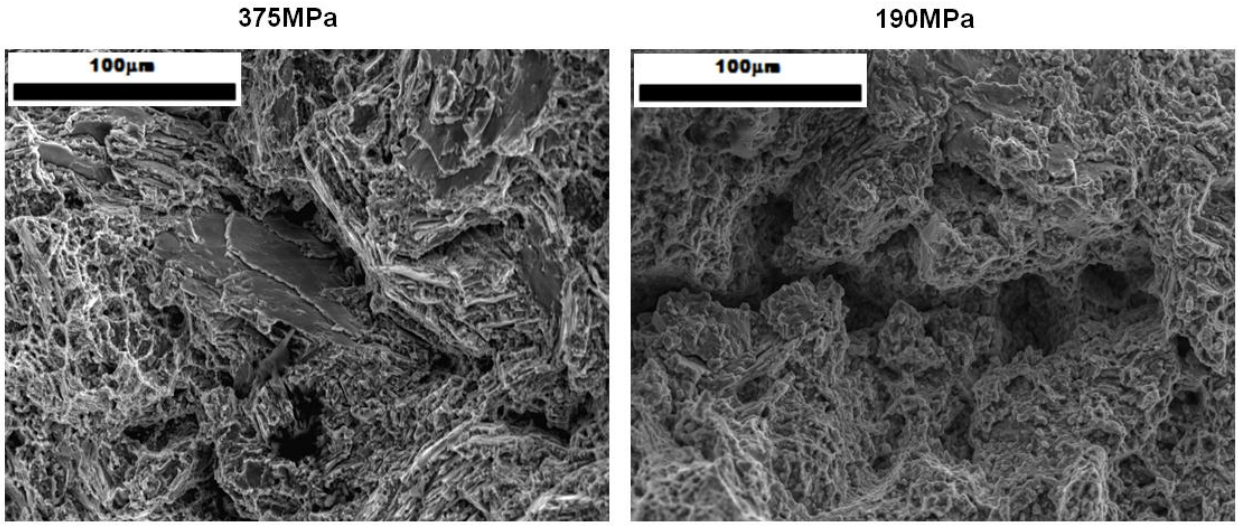

Figure 7: Scanning electron microscopy images of the samples tested at 375MPa (left) and 190MPa (right), both at 700^{o}C.

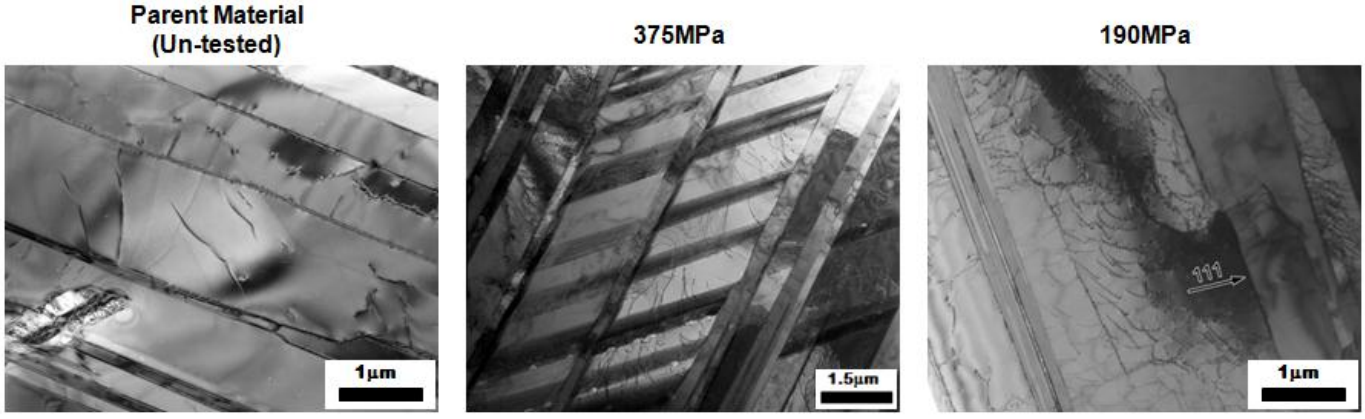

Figure 8: Transmission electron microscopy (TEM) of the parent material (left) and the two crept specimens at 375MPa (middle) and 190MPa (right).

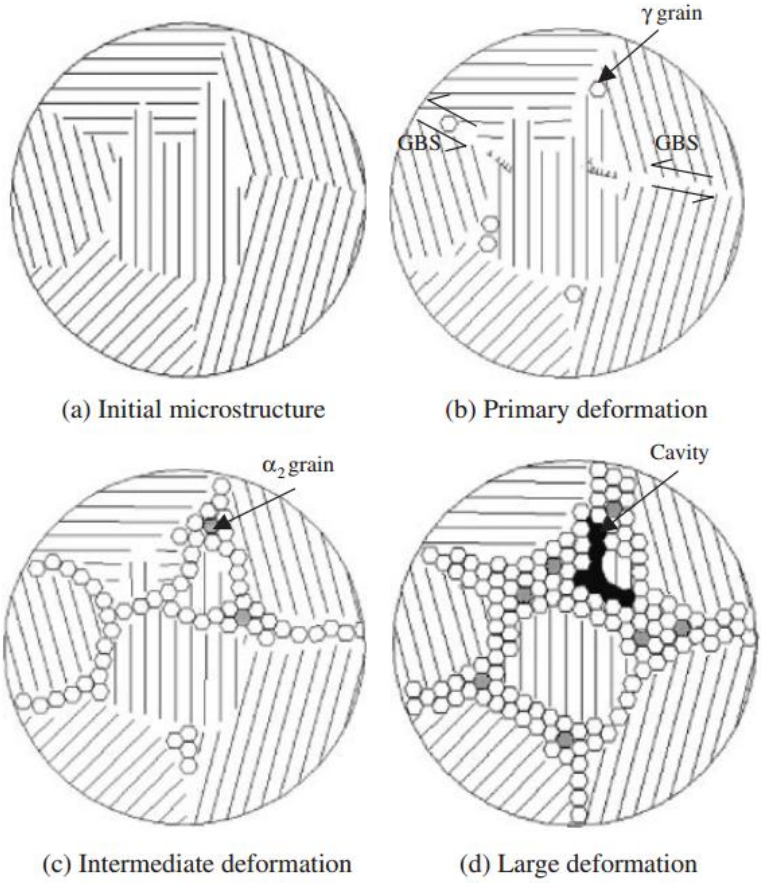

Figure 9: A model of creep deformation in TiAl alloys **(Zhu, 2004)**.